

RSC Advances



This is an *Accepted Manuscript*, which has been through the Royal Society of Chemistry peer review process and has been accepted for publication.

Accepted Manuscripts are published online shortly after acceptance, before technical editing, formatting and proof reading. Using this free service, authors can make their results available to the community, in citable form, before we publish the edited article. This *Accepted Manuscript* will be replaced by the edited, formatted and paginated article as soon as this is available.

You can find more information about *Accepted Manuscripts* in the [Information for Authors](#).

Please note that technical editing may introduce minor changes to the text and/or graphics, which may alter content. The journal's standard [Terms & Conditions](#) and the [Ethical guidelines](#) still apply. In no event shall the Royal Society of Chemistry be held responsible for any errors or omissions in this *Accepted Manuscript* or any consequences arising from the use of any information it contains.

Cite this: DOI: 10.1039/c0xx00000x

www.rsc.org/xxxxxx

ARTICLE TYPE

Self-assembling few-layer MoS₂ nanosheets on CNT backbone for high-rate and long-life lithium-ion batteries

Dayong Ren, Hao Jiang,* Yanjie Hu, Ling Zhang, Chunzhong Li*

Received (in XXX, XXX) Xth XXXXXXXXX 20XX, Accepted Xth XXXXXXXXX 20XX

DOI: 10.1039/000000x

We demonstrate the self-assembly of few-layer MoS₂ nanosheets on CNT backbone via a facile hydrothermal reaction with the subsequent annealing process. In this structure, the few-layer MoS₂ nanosheets with controllable content are alternately and vertically grown on the surface of CNTs, forming a three-dimensional hierarchical nanostructure. The optimized MoS₂/CNTs hybrids could be applied as a fascinating anode material for high-rate and long cycle life lithium ion batteries (LIBs). Compared with the commercial MoS₂ (716 mAh g⁻¹), the as-prepared MoS₂/CNTs hybrids exhibit a much higher specific capacity of 1293 mAh g⁻¹ at 200 mA g⁻¹ with remarkably enhanced rate capability (888 mAh g⁻¹ even at 3200 mA g⁻¹). More significantly, we find that MoS₂/CNTs hybrids show no capacity fading after 200 cycles at 400 mA g⁻¹. As for MoS₂-based anode materials, such overwhelming electrochemical performance endows the present MoS₂/CNTs hybrids huge potential for developing LIBs.

Introduction

Lithium-ion batteries (LIBs) have now become the predominant power source for a wide range of portable electronic devices. In recent years, the development of electric vehicles and hybrid electric vehicles has triggered an ever-increasing demand for LIBs with higher power density and long cycle life.¹⁻³ Their performances are strongly dependent on the choice of anode and cathode materials. As for anode materials, graphite is widely used as commercial anode materials in view of its natural abundance and good structural stability.⁴⁻⁶ However, it suffers from a relatively low theoretical capacity of 372 mAh g⁻¹. Therefore, it is crucial to search alternative anode materials with higher capacity and long cycle life for the development of LIBs.

As a typical layered transition metal sulfide, MoS₂ has received intense interest as a promising electrode material for LIBs because of its graphite-like structure.⁷⁻⁹ The layered structure and the weak van der Waals forces between MoS₂ layers facilitate reversible Li⁺ intercalation and extraction.¹⁰ However, like the graphene, the freshly synthesized MoS₂ layers have a tendency to aggregate during practical applications, even in the drying process, greatly reducing the electrochemical active sites. Another weakness of MoS₂ is its poor electrical conductivity. Both the two disadvantages make its rate capability and cycling stability unsatisfactory. To solve these problems, an effective approach is to hybridize MoS₂ with advanced carbon materials.¹¹⁻¹³ For example, layered MoS₂/graphene composites¹⁴ and MoS₂/amorphous carbon composites¹⁵ have been synthesized as LIBs anode materials, exhibiting an improved specific capacity with good rate and cycling performances. Notably, for the hybrid of MoS₂ and CNTs, the MoS₂ layers prefer to confine to the CNTs surface, leading to the formation of tubular MoS₂ layers

with high crystallinity.¹⁶⁻¹⁸ In this regard, a high loading mass will lower the utilization of MoS₂ active material while a low loading mass will result in low capacity based on the MoS₂/CNTs hybrids. If the MoS₂ nanosheets can be uniformly dispersed on CNTs, which will induce the coupling effect between them, which will result in remarkable enhancement of electrochemical performance.

In the present work, we demonstrate a simple route for realizing the self-assembly of few-layer MoS₂ nanosheets on CNT backbone, in which the few-layer MoS₂ nanosheets are alternately grown on the surface of CNT, forming a three-dimensional hierarchical nanostructure. The content of MoS₂ can be easily controlled simply by tuning the molybdate content. When evaluated as anode materials for LIBs, the optimized MoS₂/CNTs hybrids indicate remarkably enhanced reversible capacity (1293 mAh g⁻¹ at current density of 200 mA g⁻¹) with excellent rate and cycling performances.

Experimental

Synthesis of the MoS₂/CNT Hybrids.

20 mg of CNTs was dispersed in a mixed solution with 15 ml water, 15 ml ethanol and 2 ml oleic acid containing 1.6 g sodium oleate, 0.6 g Na₂MoO₄ and 0.8 g L-cysteine by ultra-sonication for 60 min. After that, the solution was put into a 50 mL Teflon-lined stainless steel autoclave and maintained at 180 °C for 24 h. The precipitates were filtered, washing with water and ethanol several times, and dried in a vacuum at 80 °C. Afterward, the dried samples were loaded into the tube furnace and calcined in Ar atmosphere at 550 °C for 120 min with a ramp of 2 °C_min⁻¹.

Characterization.

Structure and morphology of the as-prepared samples were characterized by X-ray diffraction (RIGAKU, D/MAX 2550 VB/PC, Japan), field emission scanning electron microscopy (Hitachi FE-S4800), transmission electron microscopy (TEM; JEOL, JEM-2100F). Thermogravimetric analysis (NETZSCHSTA409PC) was carried out with a heating rate of $10\text{ }^{\circ}\text{C min}^{-1}$ under flowing air. Fourier transform infrared (FTIR) spectra were measured by using a Nicolet 5700 spectrophotometer, in the range of 400 to 4000 cm^{-1} with a resolution of 4 cm^{-1} . N_2 adsorption/desorption was determined by Brunauer-Emmett-Teller (BET) measurements using an ASAP-2020 surface area analyzer.

Electrochemical Measurements.

LIB performance was determined using CR2016 type coin cells assembled in an argon-filled glove box. The working electrode was prepared by mixing the active material, carbon black (Super-P-Li), and a polymer binder (poly(vinylidene difluoride), PVDF, Aldrich) at a weight ratio of 7:2:1. A polypropylene film (Celgard-2400) was used as a separator. Li foil was used as the counter electrode. The electrolyte was a 1 M LiPF_6 solution in a 50:50 (w/w) mixture of ethylene carbonate (EC) and diethyl carbonate (DMC). The galvanostatic charge and discharge experiment was performed with a battery tester LAND-CT2001A in the voltage range of $0.01\text{ V} - 3.0\text{ V}$ at room temperature. The impedance spectra were recorded by applying a sine wave with amplitude of 5.0 mV over the frequency range from 100 kHz to 0.01 Hz .

Results and discussion

The few-layer MoS_2 nanosheets assembled on CNT backbone, forming a three-dimensional hierarchical nanostructure, which has been realized by a simple hydrothermal reaction of sodium molybdate and L-Cysteine in the presence of CNTs with subsequent annealing in Ar at $550\text{ }^{\circ}\text{C}$. The morphology of the products was characterized by both FESEM (Figure S1, ESI) and TEM (Figure 1a-c). As shown in low-magnification TEM image (Figure 1a), the uniform morphology of the MoS_2 nanosheets grown on CNTs have diameters of $\sim 100\text{ nm}$, while the diameter

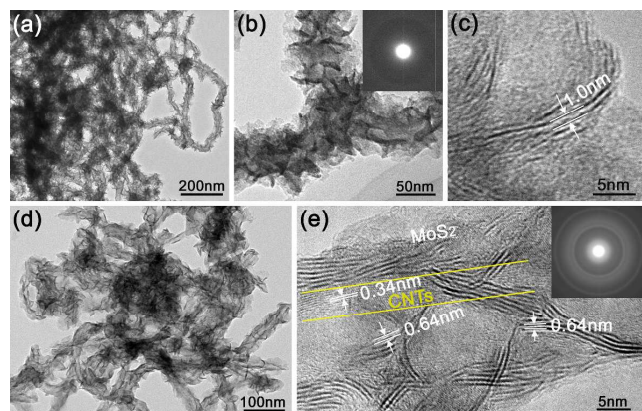


Fig. 1 (a) Low-, (b) high-magnification and (c) high-resolution TEM images of the freshly synthesized MoS_2/CNTs hybrids, inset in (b) showing the corresponding SAED pattern; (d) high-magnification and (e) high-resolution TEM images of the annealed MoS_2/CNTs hybrids at $550\text{ }^{\circ}\text{C}$ for 2 h, inset in (e) showing the corresponding SAED pattern.

of CNTs is about $\sim 20\text{ nm}$. High-magnification TEM image (Figure 1b) reveals the MoS_2 nanosheets are interconnected and vertically distributed on the surface of CNTs, forming a very intriguing three-dimensional hierarchical nanostructure. By tuning the molybdate content, the content of MoS_2 can be easily controlled without changing their morphology. More interestingly, the two layered spacing can be measured to be about 1.0 nm , which is much larger than the value of the reported MoS_2 (0.64 nm). The data is in good agreement with XRD results, as shown in Figure 2 (black line). It can be found that the (002) reflection disappears while a clear broad peak at $\sim 8.4^{\circ}$ (marked by 1#) and a poor broad peak at $\sim 16.7^{\circ}$ (marked by 2#) appear. The interlayer distance of peak 1# can be calculated to $\sim 1.0\text{ nm}$ according to the Bragg equation, which is the same as the TEM observation. Such large interlayer distance may be attributed to the presence of oleic acids on the surface of single-layer MoS_2 .¹⁹ The insertion of oleic acids into the layer of MoS_2 has been confirmed by FTIR analysis as shown Figure S2. Prior to heat treatment, the fresh MoS_2/CNTs clearly display a keen peak at 2902 cm^{-1} , which is assigned to C-H stretching vibration of CH_2 and CH_3 in oleic acids. The peak at 1706 cm^{-1} belongs to the C=O stretching vibration of COOH. The peak at 1399 cm^{-1} belongs to the vibration of $-\text{CH}=\text{CH}-$. The peak at 1040 cm^{-1} attributed to the vibration of C-O. The peak at 766 cm^{-1} to the $\delta_{\text{C-H}}$ (bending vibration), which is characteristic of $-\text{CH}_2-$ in long-chain alkanes. All the peaks disappeared after the calcination as a result of the removal of oleic acids as shown in Figure S2 (red line). In view of the strong confined effects of MoS_2 interlayer from their self-assembly process, it is hard to remove the surfactant oleic acids

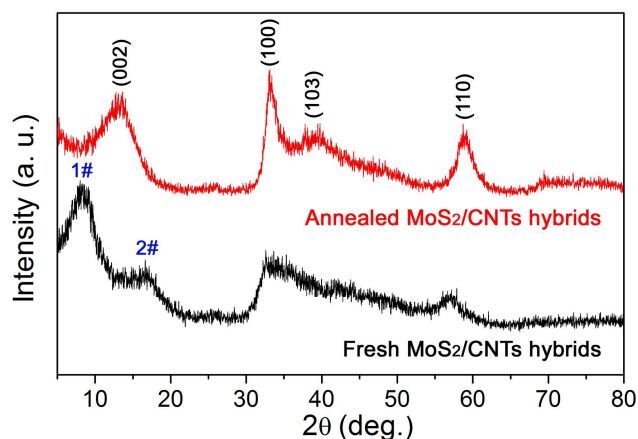


Fig. 2 XRD patterns of the annealed MoS_2/CNTs hybrids (red line) and the fresh MoS_2/CNTs hybrids (black line), respectively.

only by washing. In addition, the crystallinity of MoS_2 is also very poor from the SAED pattern in inset of Figure 1b. To totally remove the residual and improve the crystallinity, an annealing process was performed. Here, we chose $550\text{ }^{\circ}\text{C}$ as the annealing temperature considering that too high temperature will result in the formation of tubular MoS_2 on the surface of CNTs (TEM image, Figure S3 in ESI). The TEM image is shown in Figure 1d. It can be observed that the morphology has been well-maintained. Figure 1e shows the HRTEM of the interface between the CNT and MoS_2 layer. It can be observed that the few-layers MoS_2 nanosheets are interconnected and directly grown on the CNT

wall. The interlayer distance is about 0.64 nm. The corresponding SAED pattern (inset in Figure 1e) shows the obvious diffraction rings, indicating a high crystallinity of the products. These results are further confirmed by XRD measurement, as shown in Figure 2 (red line). The XRD pattern of the annealed MoS₂/CNTs hybrids displays the distinct (002), (100), (103) and (110) diffraction peaks of 2H-MoS₂ (JCPDS 37-1492). Furthermore, the annealing MoS₂/CNTs hybrids also possess a high BET surface area of 45.0 m² g⁻¹ with a bimodal mesopore size distribution (Figure S4 in ESI), which is important for achieving high energy density and power density for LIBs.

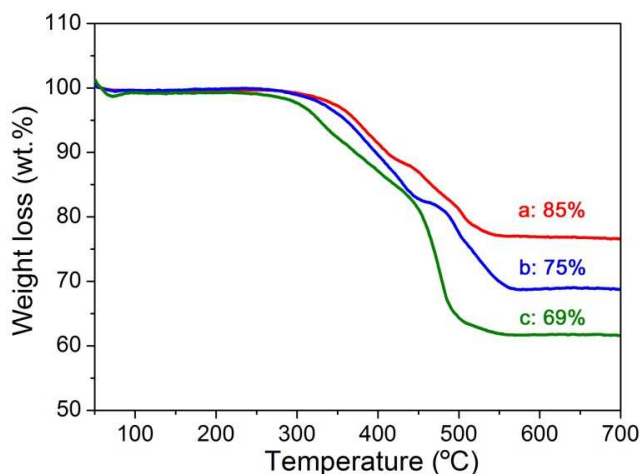


Fig. 3 TG curves of MoS₂/CNTs hybrids with different MoS₂ content, labeled as sample a-c.

To optimize the composition, the annealed MoS₂/CNTs hybrids with different MoS₂ content have been synthesized, which are determined by TG analysis. As shown in Figure 3, the weight loss was measured to be 76%, 68% and 62% for sample a-c in order. Each TG curve obviously shows two weight losses. The first weight loss occurs at about 380 °C, caused by the oxidation of MoS₂ to MoO₃.²⁰ The other weight loss occurs at about 520 °C, which can be attributed to the combustion of the CNTs. Assuming that the residual was pure MoO₃ after TG measurement, the MoS₂ content of sample a-c could be estimated to be 85%, 75% and 69%, respectively. Their electrochemical performances were preliminarily evaluated by assembling them into coin-type 2016 cells, respectively. The relationship of the annealed MoS₂/CNTs hybrids with different MoS₂ content and their electrochemical performances has been investigated in Figure S5 in ESI. It can be seen that, with the increase of MoS₂ content, a better electrochemical performance can be obtained. In this work, a maximum MoS₂ content can reach as high as ~ 85%, which then has been further evaluated in detail.

Their structure and morphology of the hybrids with 85% MoS₂ content have already been characterized in detail before. For convenient discussion, the corresponding hybrids are labelled as MoS₂/CNTs hybrids in the subsequent text. Figure 4a shows the cyclic voltammograms (CVs) of the MoS₂/CNTs hybrids within a potential range of 0.01 V - 3 V. As shown in Figure 4a, two peaks at ~ 0.9 V and ~ 0.45 V are observed in the 1st cathodic sweep. The peak at ~ 0.9 V is attributed to the intercalation of Li ion into MoS₂ lattice to form Li_xMoS₂²¹ and the other peak at ~ 0.45 V

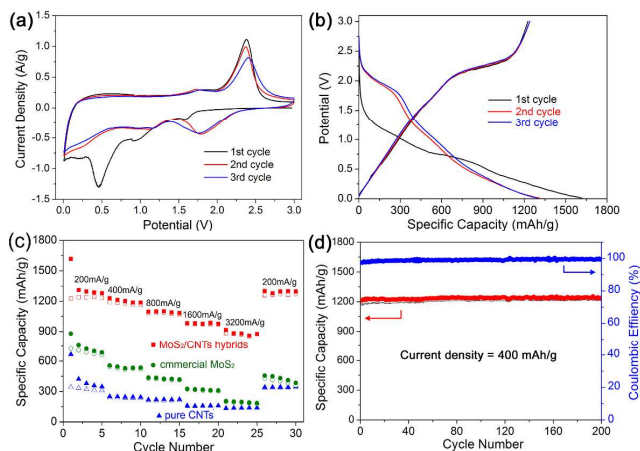


Fig. 4 (a) CV curves at a scan rate of 0.2 mV s⁻¹ for the initial 3 cycles, (b) charge-discharge curves at 200 mA g⁻¹ for the initial 3 cycles of the MoS₂/CNTs hybrids, (c) rate capabilities of the MoS₂/CNTs hybrids and the commercial MoS₂, respectively, (d) cycling behavior and Coulombic efficiency of the MoS₂/CNTs hybrids at a current density of 400 mA g⁻¹.

corresponds to the decomposition reaction of Li_xMoS₂ to Mo and Li₂S.²¹ In addition, another poor peak at 1.6 V can also be observed, which could be attributed to the reduction reaction of the oxygen-containing functional groups from CNTs.²² In the reverse anode sweep, a weak peak at 1.7 V appears owing to the incomplete oxidation of Mo metal.²³ The strong peak at 2.4 V can be assigned to the delithiation of Li₂S.²³ In the subsequent 2nd and 3rd cathodic sweeps, two peaks are observed at 1.8 V and 1.2 V, respectively, mainly due to the following two reactions: 2Li⁺ + S + 2e⁻ → Li₂S and xLi⁺ + xe⁻ → Li_xMoS₂.²³ Fig 4b exhibits the initial three discharge-charge profiles in the potential range of 0.01 V - 3 V at current density of 200 mA g⁻¹. The initial discharge and charge capacities can reach 1617 mAh g⁻¹ and 1226 mAh g⁻¹, respectively, showing a remarkably enhanced Coulombic efficiency of 75.8% thanks to the unique nanostructure assembled by few-layered MoS₂ nanosheets on CNTs. In the next two discharge and charge processes, the discharge capacity can still reach 1310 mAh g⁻¹ and 1296 mAh g⁻¹ with Coulombic efficiency as high as 95% and 96%, respectively, demonstrating a high reversible capacity and excellent cycling stability.

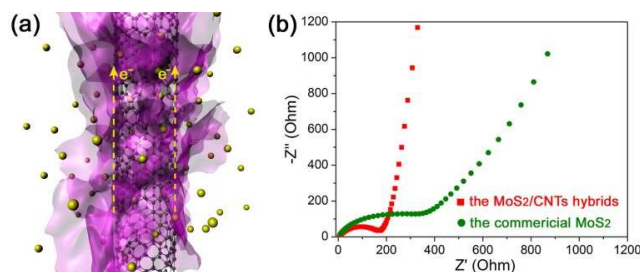


Fig. 5 (a) Scheme illustration of the diffusion of electron and Li ion for the as-prepared MoS₂/CNTs hybrids, (b) Nyquist plots of the MoS₂/CNTs hybrids and the commercial MoS₂, respectively.

The rate capability of the MoS₂/CNTs hybrids was further evaluated, as shown in Figure 4c. The average discharge capacities are 1293 mAh g⁻¹, 1203 mAh g⁻¹, 1092 mAh g⁻¹, 983 mAh g⁻¹ and 888 mAh g⁻¹ at current densities of 200 mA g⁻¹, 400 mA g⁻¹, 800 mA g⁻¹, 1600 mA g⁻¹ and 3200 mA g⁻¹, respectively. After the rapid charge and discharge at 3200 mA g⁻¹, a mean capacity of 1294 mAh g⁻¹ can be recovered when the current

density returns back to 200 mA g⁻¹. For comparison, the commercial MoS₂ was also tested under the same condition, showing much lower capacity of 716 mAh g⁻¹ at 200 mA g⁻¹, with poor rate performance (the capacity of only 192 mAh g⁻¹ at 3200 mA g⁻¹). Such high specific capacity and rate capability are superior or comparable at least to the best results reported for MoS₂-based electrode materials.^{12-15,24-27} Very recently, Yang et al.²⁴ reported the synthesis of hierarchical MoS₂/polyaniline nanowires which showed an intriguing specific capacity of 1062.7 mAh g⁻¹ at 200 mA g⁻¹ with ~ 30% capacity retention at 1000 mA g⁻¹, but still lower than our samples (1293 mAh g⁻¹ at 200 mA g⁻¹ with 888 mAh g⁻¹ capacity retention even at 3200 mA g⁻¹). After testing the rate performance, the MoS₂/CNTs hybrids subsequently continue to be evaluated at a current density of 400 mA g⁻¹ for another 200 cycles (Figure 4d). The hybrids show no capacity fading in the whole cycling process and deliver high specific capacity of ~ 1200 mAh g⁻¹ with a Coulombic efficiency of ~ 100%. The outstanding cycling stability would overwhelm the MoS₂-based anode materials in the literature, such as three-dimensional tubular architectures assembled by single-layered MoS₂ (73.8% capacity retention after 50 cycles),²⁸ hierarchical MoS₂/polyaniline nanowires (89.6% capacity retention after 50 cycles)²⁴ and MoS₂/amorphous carbon composites (95% capacity retention after 100 cycles).¹⁵ In a previous work, Chen et al.¹² reported the synthesis layered MoS₂/graphene composites, showing almost no capacity loss (1187 mAh g⁻¹ at 100 mA g⁻¹) after 100 cycles (1200 mAh g⁻¹ at 400 mA g⁻¹ after 200 cycles for our samples). Such excellent electrochemical performance is mainly attributed to the unique hierarchical nanostructure. As shown in Figure 5a, the introduction of CNTs builds high-speed conductive channel for MoS₂ nanosheets, greatly boosting the rapid electron transfer during Li ion insertion/extraction. To verify this viewpoint, the electrochemical impedance spectra of the MoS₂/CNTs hybrids and the commercial MoS₂ were performed. As shown in Figure 5b, the MoS₂/CNTs hybrids demonstrate a much lower resistance (~ 183.5 Ω) than the commercial MoS₂ (~ 541.6 Ω). On the other hand, the few-layer MoS₂ nanosheets were firmly and alternately assembled on the CNTs, which provided high structural sufficient electrochemical active sites and therefore resulting in high stability and meanwhile created amounts of porous configuration. The Li ion from the surrounding of MoS₂/CNTs have significantly improved contact with the Li accommodate layers, ensuring specific capacity and rate performance.

Conclusions

In conclusion, we have successfully realized the self-assembly of few-layer MoS₂ nanosheets on CNT backbone via a facile hydrothermal reaction with subsequent annealing process. In this structure, the few-layer MoS₂ nanosheets were alternately and vertically grown on the surface of CNTs forming a three-dimensional hierarchical nanostructure. The MoS₂ content can be easily controlled with a maximum content of 85%. Such MoS₂/CNTs hybrids could be applied as an intriguing anode material for the development of LIBs with high rate capability and long cycle life. Compared with the commercial MoS₂ (716 mAh g⁻¹ at 200 mA g⁻¹), the as-prepared MoS₂/CNTs hybrids demonstrated a much higher specific capacity of 1293 mAh g⁻¹ at

200 mA g⁻¹ with remarkably enhanced rate capability (888 mAh g⁻¹ even at 3200 mA g⁻¹). More significantly, they also possess a very high cycling stability, i.e. almost no capacity loss after over 200 cycles at 400 mA g⁻¹. Such overwhelming electrochemical performance endows the MoS₂/CNTs hybrids huge potential as an anode material for LIBs.

Acknowledgements

This work was supported by the National Natural Science Foundation of China (51173043, 21236003, 21322607), the Special Projects for Nanotechnology of Shanghai (11nm0500200), the Basic Research Program of Shanghai (13JC1408100), Program for New Century Excellent Talents in University (NCET-11-0641), the Fundamental Research Funds for the Central Universities.

Notes and references

- ^a Key Laboratory for Ultrafine Materials of Ministry of Education, School of Materials Science and Engineering, East China University of Science and Technology, 130 Meilong Road, Shanghai 200237, China, Email: jianghao@ecust.edu.cn, czli@ecust.edu.cn; Fax: +86 21 64250624; Tel: +86 21 64250949
- Electronic Supplementary Information (ESI) available: [details of any supplementary information available should be included here]. See DOI: 10.1039/000000x/
- 1 M. Armand, J. M. Tarascon, *Nature* 2008, **451**, 652-657.
 - 2 M. Winter, R.J. Brodd, *Chem. Rev.* 2004, **104**, 4245-4270.
 - 3 S.J. Guo, S.J. Dong, *Chem. Soc. Rev.* 2011, **40**, 2644-2672.
 - 4 R. Mukherjee, R. Krishnan, T.M. Lu, N. Koratkar, *Nano Energy* 2012, **1**, 518-533
 - 5 X. Cao, Y. Shi, W. Shi, X. Rui, Q. Yan, J. Kong, H. Zhang, *Small* 2013, **9**, 3433-3438
 - 6 F. Lin, D. Nordlund, I. M. Markus, T. Weng, H. L. Xin, M. M. Doeff, *Energy Environ. Sci.* 2014, DOI: 10.1039/c4ee01400f.
 - 7 J. Xiao, D. Choi, L. Cosimbescu, P. Koech, J. Liu, J. P. Lemmon, *Chem. Mater.* 2010, **22**, 4522-4524.
 - 8 H. Hwang, H. Kim, J. Cho, *Nano Lett.* 2011, **11**, 4826-4830.
 - 9 J. Xiao, X.J. Wang, X.Q. Yang, S.D. Xun, G. Liu, P.K. Koech, J. Liu, J.P. Lemmon, *Adv. Funct. Mater.* 2011, **21**, 2840-2846.
 - 10 A.V. Murugan, M. Quintin, M.H. Delville, G. Campet, C.S. Gopinath, K. Vijayamohan, *J. Power Sources* 2006, **156**, 615-619.
 - 11 H. Jiang, P.S. Lee, C.Z. Li, *Energy Environ. Sci.* 2013, **6**, 41-53.
 - 12 K. Chang, W.X. Chen, *ACS Nano* 2011, **5**, 4720-4728.
 - 13 Y.M. Shi, Y. Wang, J.I. Wong, A.Y.S. Tan, C. L. Hsu, L.J. Li, Y.C. Lu, H.Y. Yang, *Sci. Rep.* 2013, **3**, 2169-2176.
 - 14 G.H. Huang, T. Chen, W.X. Chen, Z. Wang, K. Chang, L. Ma, F.H. Huang, D.Y. Chen, J.Y. Lee, *Small* 2013, **9**, 3693-3703.
 - 15 K. Chang, W.X. Chen, L. Ma, H. Li, H. Li, F.H. Huang, Z.D. Xu, Q.B. Zhang, J.Y. Lee, *J. Mater. Chem.* 2011, **21**, 6251-6257.
 - 16 V.O. Koroteev, L.G. Bulusheva, I.P. Asanov, E.V. Shlyakhova, D.V. Vyalikh, A.V. Okotrub, *J. Phys. Chem. C* 2011, **115**, 21199-21204.
 - 17 L. Ma, W.X. Chen, Z.D. Xu, J.B. Xia, X. Li, *Nanotechnology* 2006, **17**, 571-574.
 - 18 Q. Wang, J.H. Li, *J. Phys. Chem. C* 2007, **111**, 1675-1682.
 - 19 K. Zhang, L. Mao, L.L. Zhang, H.S.O. Chan, X.S. Zhao, J.S. Wu, *J. Mater. Chem.* 2011, **21** 7302-7307.
 - 20 S.K. Park, S.H. Yu, S. Woo, B. Quan, D.C. Lee, M.K. Kim, Y.E. Sung, Y.Z. Piao, *Dalton Trans.* 2009, **42**, 2399-2405.
 - 21 E. Benavente, M.A. Santa Ana, F. Mendizábal, G. González, *Coord. Chem. Rev.* 2002, **224**, 87.
 - 22 K. Chang, W.X. Chen, *J. Mater. Chem.* 2011, **21**, 17175-17184.
 - 23 X.P. Fang, X.Q. Yu, S.F. Liao, Y.F. Shi, Y.S. Hu, Z.X. Wang, G.D. Stucky, L.Q. Chen, *Microporous Mesoporous Mater.* 2012, **151**, 418-423.

-
- 24 L.C. Yang, S.N. Wang, J.J. Mao, J.W. Deng, Q.S. Gao, Y. Tang, O.G. Schmidt, *Adv. Mater.* 2013, **25**, 1180-1184.
- 25 H.J. Zhang, K.X. Wang, X.Y. Wu, Y.M. Jiang, Y.B. Zhai, C. Wang, X. Wei, J.S. Chen, *Adv. Funct. Mater.* 2014, DOI: 10.1002/adfm.201303856.
- 5 26 X. Zhou, L.J. Wan, Y.G. Guo, *Chem. Commun.* 2013, 49, 1838-1840.
- 27 P.P. Wang, H.Y. Sun, Y.J. Ji, W.H. Li, X. Wang, *Adv. Mater.* 2014, **26**, 964-969.
- 10 28 Z. Wang, T. Chen, W.X. Chen, K. Chang, L. Ma, G.C. Huang, D.Y. Chen, J.Y. Lee, *J. Mater. Chem. A* 2013, **1**, 2202-2210.

TOC

